ACS APPLIED NANO MATERIALS

www.acsanm.org Article

Graphene-Based Transparent Conducting Substrates for GaN/AlGaN Nanocolumn Flip-Chip Ultraviolet Light-Emitting Diodes

Andreas Liudi Mulyo, Anjan Mukherjee, Ida Marie Høiaas, Lyubomir Ahtapodov, Tron Arne Nilsen, Håvard Hem Toftevaag, Per Erik Vullum, Katsumi Kishino,* Helge Weman, and Bjørn-Ove Fimland*

Cite This: *ACS Appl. Nano Mater.* 2021, 4, 9653−9664 Read Online

ACCESS | Metrics & More | Article Recommendations | Supporting Information

ABSTRACT: Flip-chip ultraviolet light-emitting diodes based on self-assembled GaN/AlGaN nanocolumns have been fabricated, exploiting single-layer graphene not only as a growth substrate but also as a transparent conducting electrode. High crystalline quality of the nanocolumns is confirmed by detailed electron microscopy characterization, also showing the intrinsic GaN quantum disk in the active region of the nanocolumns. These features are further confirmed in the optical emission, where the absence of defect-related yellow emission and the presence of blue-shifted (from the usual 365 nm band gap emission of bulk wurtzite GaN) emission at ∼350 nm, ascribed to quantum confinement and strain effects, are observed. Despite a noticeable graphene damage after the nanocolumn growth that causes high sheet resistance of graphene and high turn-on voltage, the proof of concept of single-layer graphene used as the transparent conducting substrate for a nanocolumn device is demonstrated. This study offers an alternative platform for the fabrication of next-generation nano-optoelectronic and electronic devices.

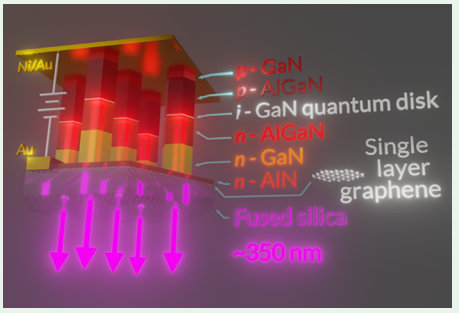

KEYWORDS: *nanocolumns, nanowires, GaN/AlGaN, graphene, light-emitting diodes, molecular beam epitaxy*

INTRODUCTION

Inorganic III-nitride semiconductor nanowires or nanocolumns represent a class of an essential nanostructure that can be exploited as the building blocks for diverse nano-electronic and nano-optoelectronic devices, including solar cells,[1,2] solar water-splitting devices,[3] transistors,[4,5] photodetectors,[6,7] lasers,[8,9] and light-emitting diodes (LEDs).[10−14] With a high surface-to-volume-ratio and nanoscale footprint, such a quasi-one-dimensional structure can accommodate greater elastic strain compared to the planar structure and suppress the formation of misfit dislocations provided that its radius is below certain nanocolumn critical values.[15] If any defect and/or dislocation is generated, they will be directed to the nanocolumn sidewalls[16] instead of vertically propagating along the [0001] growth direction, leaving the active area of the nanocolumn defect-free. Utilizing the nanocolumn structure can thus alleviate the uncompromising lattice match requirement in the thin-film structure in order to obtain a semiconductor material with high crystalline quality.

Such conditions wherein a global epitaxial relationship between III-nitride nanocolumns and substrates is not necessarily vital can in principle facilitate the realization of monolithic integration of highly lattice-mismatched materials. In other words, nanocolumns can be grown on virtually any kind of substrates, and among these are amorphous materials and other non-conventional substrates, which can even provide alternative and low-cost options for commercialization. This is evidenced by the fact that the investigations of III-nitride nanocolumn synthesis not only have been extensively conducted on crystalline substrates[17−21] but also have been attempted on Ti,[22,23] Mo,[24,25] MoS_2,[26] Ta,[22] Ti_3C_2,[27] diamond,[28] h-BN,[29] Al_xO_y,[30] and glass.[31−34] Going beyond the aforementioned materials, the proposition of utilizing two-dimensional materials as the substrate for nanocolumns may offer a unique approach in attaining greater flexibility and functionalities in future device configurations. So far, the formation of vertical III-nitride nanocolumns has been exclusively demonstrated on graphene,[35−47] but the importance of other two-dimensional materials,[48] such as single- or few-layer MoS_2, Ti_3C_2, and h-BN, as a substrate cannot be ignored, considering their distinct properties that can be favorable for a wide range of devices. (Please note that the previously mentioned MoS_2,[26] Ti_3C_2,[27] and h-BN[29] substrates for nanocolumn growth have thicknesses of 60, 19.2, and 3 nm, respectively. They are much thicker as compared to their single-layer counterparts that are experimentally determined to

Received: July 19, 2021
Accepted: August 4, 2021
Published: August 18, 2021

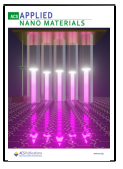

Scheme 1. Substrate Preparation and Subsequent GaN/AlGaN Nanocolumn Synthesis

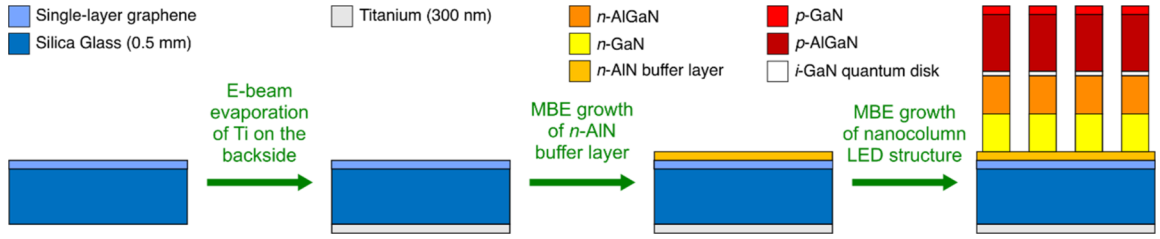

have thicknesses of 0.80−0.86, 1.7−2.0, and 0.38−0.45 nm for MoS_2,[49,50] Ti_3C_2,[51] and h-BN,[49,52] respectively).

From the perspective of III-nitride nanocolumn-based devices, graphene[53] has some specific benefits over h-BN[52] and MoS_2[54] as a growth substrate since it is stable during high synthesis temperatures and due to its potential as a transparent conducting electrode. This is especially important for the development of optoelectronic devices operating in the ultraviolet (UV) ranges. Despite these opportunities, only a couple of studies have reported the integration of graphene in functional working UV devices, including photodetectors based on InGaN nanorods on tri-layer graphene[41] and LEDs in a flip-chip configuration based on GaN/AlGaN nanocolumns on double-layer graphene.[40] However, an optoelectronic device exploiting single-layer graphene has yet to be demonstrated. Additionally, the usage of single-layer graphene could be more beneficial compared to multiple graphene layers because it has higher transparency across the UV and visible spectrum.[55] Specifically for the UV-C region, where specific wavelength ranges ∼270 nm can be utilized for disinfection of viruses and bacteria, graphene absorbs ∼8% of the incoming light for each layer.[55]

In this work, a slightly inverse-tapered III-nitride nanocolumn flip-chip LED structure on a *single-layer* graphene substrate is documented. Self-assembly of a vertical n-GaN/n-AlGaN/i-GaN quantum disk/p-AlGaN/p-GaN nanocolumn LED structure was synthesized on the graphene substrate using radio-frequency plasma-assisted molecular beam epitaxy (RF-PAMBE). At the very start of the growth, an n-AlN buffer layer was formed to achieve a high density of n-GaN nanocolumn growth. The grown nanocolumn device structure exhibits high crystalline quality that is comparable with that of existing studies using graphene or other materials as substrates. The flip-chip UV LED structure based on this hybrid system was realized by employing graphene simultaneously as a substrate and a bottom electrode, that is, a *transparent conducting substrate*. The LED device has an emission wavelength at ∼350 nm, which likely originates from the intrinsic GaN quantum disk.

EXPERIMENTAL SECTION

The graphene utilized in this work was commercially available (single-layer) graphene with a surface area of 10 × 10 mm^2 provided by Graphene Platform Corp. (Tokyo, Japan). It was synthesized using a standard chemical vapor deposition technique on a Cu foil,[56] which was subsequently transferred onto the center of a 2 in. fused silica glass substrate (0.5 mm thick) acting as a host carrier for the graphene. Before insertion into the MBE system for nanocolumn growth on the graphene, a 300 nm-thick Ti layer was deposited by e-beam evaporation on the backside of the fused silica substrate to obtain efficient and uniform absorption of thermal radiation from the heater to the substrate (Scheme 1). Additionally, this Ti layer enables a pyrometer reading of the substrate temperature during the growth.

Self-assembled GaN/AlGaN nanocolumn heterostructures were grown without a catalyst using an EpiQuest RF-PAMBE system (Sophia University) under N-rich conditions, where the growth chamber is equipped with standard solid-source Knudsen cells: Al and Ga effusion cells to provide Al and Ga atoms, respectively; Si and Mg effusion cells for the supply of Si and Mg dopant atoms, respectively; and an RF nitrogen plasma source to generate active nitrogen. A thin n-AlN buffer layer and the nanocolumn LED structure were then grown similarly as described in our previous report (Scheme 1)[40] but with a few notable differences, see Table S1: (i) a short n-AlGaN segment was grown on the n-GaN template; (ii) an i-GaN quantum disk layer was introduced as the active layer; and (iii) p-AlGaN and p-GaN sections were formed at a higher substrate temperature for suppressing the coalescence at the top part of the nanocolumns. The resulting nanocolumn structure should nominally consist of 140 nm n-GaN, 130 nm n-AlGaN, 5 nm i-GaN quantum disk, 180 nm p-AlGaN, and 34 nm p-GaN, having a total length of 489 nm.

The surface morphology, density, and size distribution of the as-grown GaN/AlGaN nanocolumn samples were studied by scanning electron microscopy (SEM) using an SII SMI3050SE focused ion beam (FIB)−SEM system and a Hitachi SU8000 SEM system at acceleration voltages of 15 and 10 kV, respectively. In addition, the composition of the as-grown GaN/AlGaN nanocolumns was assessed using high-resolution X-ray diffraction (HRXRD) with a Bruker D8 Discovery high-resolution diffractometer (Cu Kα source whose wavelength is 1.5406 Å) using 0.2 mm anti-scatter slits in front of the detector.

Structural details of the individual GaN/AlGaN nanocolumns, along with the interfacial properties between nanocolumns, AlN buffer layer, graphene, and fused silica glass support were investigated by means of high-resolution transmission electron microscopy (HRTEM) using a double-Cs-corrected cold field emission gun JEOL ARM200F operating at 200 kV. Additionally, this instrument is equipped with a Centurio SDD and a QuantumER GIF for energy-dispersive X-ray spectroscopy (EDS) and electron energy loss spectroscopy (EELS), respectively. Simultaneous EDS and EELS were carried out in the scanning TEM (STEM) mode to obtain chemical compositional analysis. Prior to these studies, the sample was coated with Pt−Pd metal using a sputter coater to avoid charging during TEM sample preparation. Cross-sectional TEM lamella was prepared using a FEI Helios G4 UX-dual-beam FIB−SEM instrument: 30 kV ion-beam acceleration voltage was employed for the coarse (initial) thinning, which was continued with 5 kV and finally 2 kV for minimizing Ga implantation and surface amorphization.

Optical properties of the as-grown GaN/AlGaN nanocolumns were examined by room temperature and low-temperature photoluminescence spectroscopy. The third harmonic of a tunable, pulsed Ti:Sapphire laser with a wavelength of ∼260 nm and pulse duration of ∼120 fs was utilized as the excitation source. The laser beam was focused on the sample using a reflective microscope objective with 50× magnification, 0.35 numerical aperture, and 5 mm focal length. The beam was widened in order to overfill the back focal aperture of the objective, resulting in a diffraction-limited spot size of ∼0.9 μm. Low-temperature optical measurements were performed by isolating the sample inside a continuous-flow liquid He cryostat, equipped with a sample heater and thermometer for precise sample temperature control. The detection of the photoluminescence signal was done using a HORIBA Jobin-Yvon spectrograph (300 lines/mm, grating

https://doi.org/10.1021/acsanm.1c02050
ACS Appl. Nano Mater. 2021, 4, 9653−9664

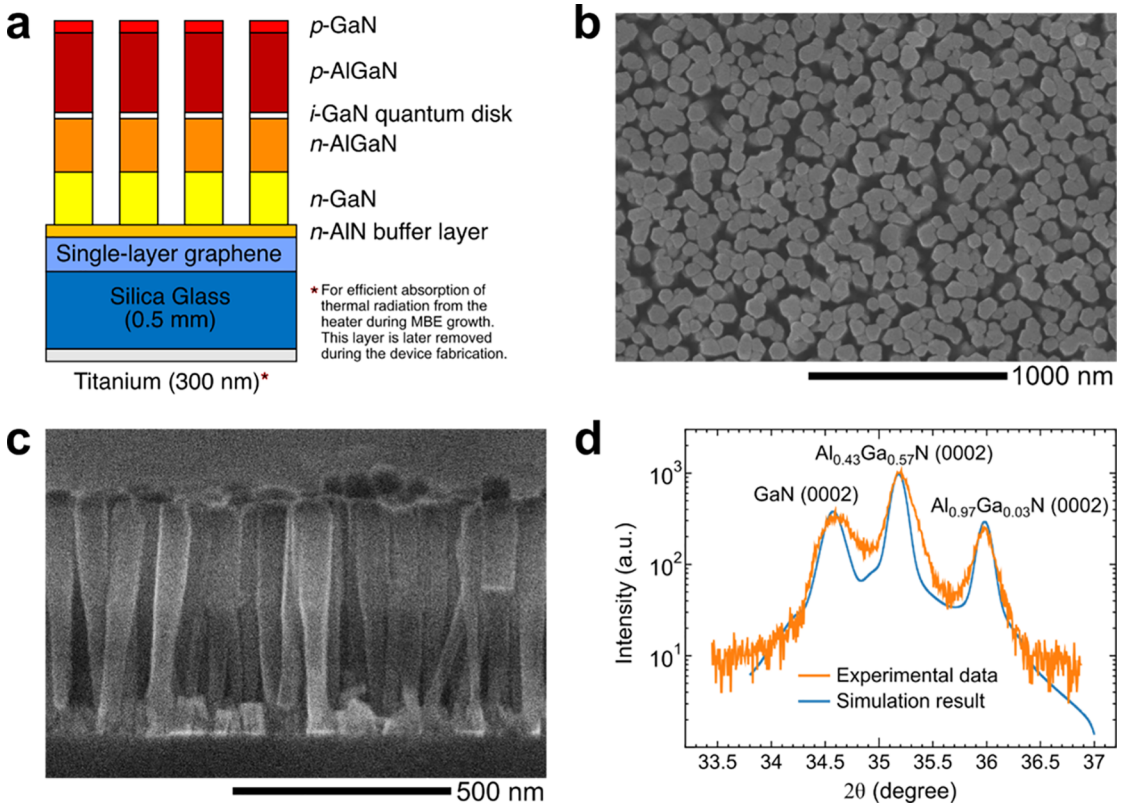

Figure 1. (a) Schematic diagram of the GaN/AlGaN nanocolumns grown on graphene, intermediated using a two-stage n-AlN buffer layer deposition method. (b,c) Representative top-view and cross-sectional SEM images of the nanocolumns on graphene, respectively. (d) HRXRD 2θ–ω scan of the GaN/AlGaN nanocolumns, showing GaN(0002), low-Al content AlGaN(0002), and high-Al content AlGaN(0002) peaks at 34.56, 35.18, and 35.98°, respectively.

blazed at 500 nm), which disperses the signal onto an UV-B-enhanced Andor Newton electron multiplying charge-coupled device detector.

Graphene properties before and after the nanocolumn growth were characterized using micro-Raman spectroscopy with a Renishaw InVia Reflex spectrometer system equipped with a 532 nm (5 and 10 mW) excitation laser. The measurements were conducted at room temperature in the backscattering configuration with a 50× or 100× objective lens. A pristine graphene sheet transferred onto fused silica glass was utilized as a comparison to graphene samples after nanocolumn growth.

In order to fabricate electrical contacts to both the top p-GaN part of the nanocolumns and the bottom graphene substrate electrode separately, an ∼15 nm thin aluminum oxide (Al_xO_y) conformal dielectric layer was deposited to the as-grown structure through atomic layer deposition. A better isolation between the two electrical contacts can be achieved by this Al_xO_y layer, leading to a reduction in the leakage current, which is essential for the realization of a better device performance. A diluted photoresist (S1813) layer was subsequently used to fill the tiny gap between the nanocolumns, where the resist was subsequently etched back using low-power oxygen plasma ashing to expose the top of the (Al_xO_y-covered) nanocolumns. The Al_xO_y layer at the top of the nanocolumns was then removed using reactive ion etching, while the Al_xO_y layer on the side wall of the nanocolumns and the graphene in the interspace between the nanocolumns were being protected by the resist layer. Since this resist layer potentially can absorb the UV light emitted from the nanocolumns, it was removed after the successful area-selective etching of the Al_xO_y layer.

A circular device aperture of ∼50 μm diameter was then defined by photolithographic processes, where a Ni (10 nm)/Au (200 nm) metal stack was deposited to form an ohmic contact to the top p-GaN part of the nanocolumns through sputtering and e-beam evaporation.[40] In order to complete the LED device structure, an ohmic and low-resistive bottom contact was then formed on the graphene layer by depositing 200 nm Au,[57] as described in our earlier work.[40] Note that the Ti layer on the backside of the fused silica support was removed before Al_xO_y deposition through mechanically assisted wet etching in a 5% diluted hydrofluoric acid solution. Scheme S1 in the Supporting Information illustrates the LED fabrication procedure (see also Figure 4.9 in ref 58). Current–voltage (I–V) characteristics of the fabricated LED devices were then measured using a Keithley 2400 source meter under dark room conditions, and the emitted electroluminescence spectra collected through the bottom substrate were then recorded as a function of the injected current level using a UV-sensitive spectrometer coupled with a fiber/cosine corrector.

RESULTS AND DISCUSSION

The design of the nanocolumn LED structure grown on graphene is given in Figure 1a, and the morphology of the grown nanocolumns is presented in Figure 1b,c, depicting top-view and cross-sectional SEM images, respectively. Since high substrate temperatures were used to form the p-AlGaN and p-GaN sections, the coalescence in the top part of the nanocolumns is not as pronounced as observed in our previous work.[40] In that work, low growth temperatures were intentionally applied to merge the upper part of the nanocolumns, aiding the formation of a continuous and flat metal contact to the top p-GaN segment during the LED processing. However, due to the nature of random growth, these nanocolumns are non-uniform in terms of size, morphology, and twist/tilt in crystal orientation. It is anticipated that such coalescence might produce structural defects, including strain and threading dislocations within the boundary of the nanocolumn.[59,60]

https://doi.org/10.1021/acsanm.1c02050
ACS Appl. Nano Mater. 2021, 4, 9653–9664

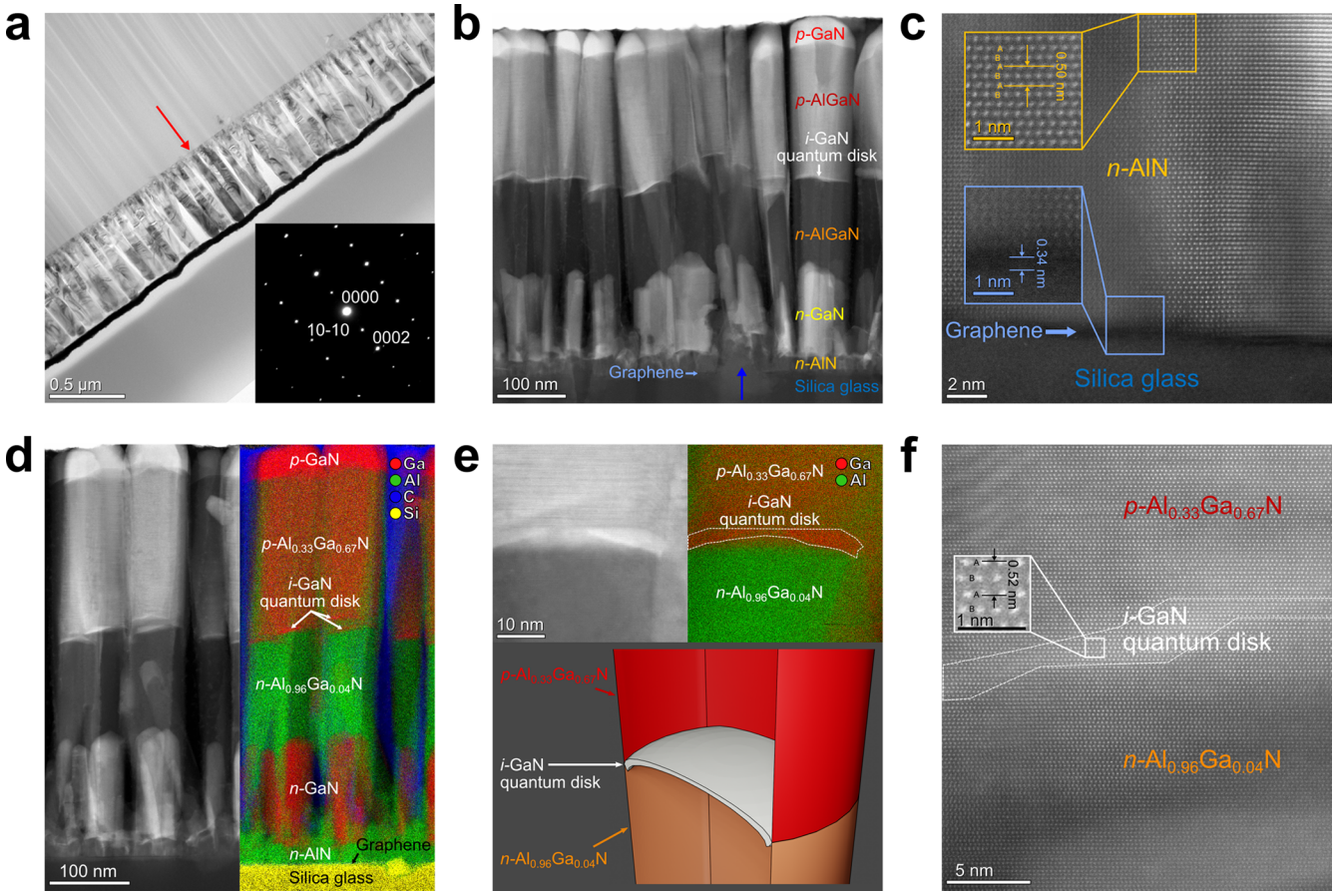

Figure 2. (a) BFTEM and (b) HAADF STEM images of the GaN/AlGaN nanocolumns grown on graphene. The red arrow in (a) points at a nanocolumn for which the electron beam is parallel to the [1−210] crystal direction (inset: corresponding electron diffraction pattern). The blue arrow in (b) indicates a region with a diffuse interface between the nanocolumns and the substrate. (c) High-resolution HAADF STEM image of the interface between the n-AlN buffer layer, graphene, and silica glass (inset: [top] wurtzite AlN crystal stacking order and [bottom] magnified graphene interface region). (d,e) HAADF STEM images and elemental mappings of a different [from what is shown in (b)] GaN/AlGaN nanocolumn area and an i-GaN quantum disk region, respectively. The bottom image in (e) illustrates the general interpretation of the i-GaN quantum disk shape. (f) High-resolution HAADF STEM image of the left side of the i-GaN quantum disk area depicted in (e) (the inset shows the wurtzite crystal stacking order of the i-GaN quantum disk).

Figure 1b demonstrates the formation of GaN/AlGaN nanocolumns with a near-hexagonal geometry in the cross-section, showing an average top diameter of 67 ± 10 nm and a density of 7.8 × 10^9 cm^{-2}. Other characteristics of these nanocolumns can be further examined in Figure 1c, showing a relatively uniform height with an average of 529 ± 10 nm (measured from the n-AlN buffer layer), along with an average bottom diameter of 40 ± 7 nm. The height of these low-angle inverse-tapered nanocolumns is half that of the preceeding nanocolumns grown on double-layer graphene[40] due to the significant reduction in growth time of the n-AlGaN and p-AlGaN sections. Additional SEM images are provided in Figure S1, showing highly dense and vertically oriented nanocolumns on the graphene substrate. Highlighted in Figure S1b is a protruding continuous structure at the base of the nanocolumns, assumed to be the n-AlN buffer layer (which can be seen later in STEM images in Figure 2).

Note that the n-AlN buffer deposition method that has been previously used,[35,39,43] namely, migration-enhanced epitaxy, is incapable of promoting high yield of vertical nanocolumn growth, as shown in the SEM images in Figure S2, possibly due to the inadequacy in providing nucleation sites for the growth of short- and high-density n-GaN nanocolumns. Only n-GaN formed on n-AlN islands[35,43] and n-AlN nanostructures can be grown with a high degree of verticality, while that formed directly on graphene grows in more random directions.[43] A *two-stage* n-AlN buffer deposition method is therefore introduced to increase the probability in obtaining vertical growth of nanocolumns (the SEM images and the details are presented in Figure S3). The uninterrupted Al deposition in the initial stage before the graphene is exposed to N atoms presumably can lead to a larger coverage of the n-AlN buffer layer on graphene. As a result, the likelihood of n-GaN directly nucleating on n-AlN is enhanced, inducing nanocolumn growth perpendicular to the graphene substrate.

The average composition of each axial nanocolumn segment for the as-grown vertical GaN/AlGaN nanocolumn ensemble was investigated using HRXRD scans. Errors in the detector angle were corrected by measuring the position of both (0002) and (0004) reflections of the strongest AlGaN peak, as there is no known substrate peak. The orange curve in Figure 1d shows the experimental data for a HRXRD scan, and the blue curve shows the result of a simulation performed using X-ray utilities developed by Kriegner et al.[61] based on the layer structure found in an EDS line scan of a single nanocolumn by TEM (discussed later). It should be noted that the purpose of this

https://doi.org/10.1021/acsanm.1c02050
ACS Appl. Nano Mater. 2021, 4, 9653−9664

simulation is to find the Al content of the GaN/AlGaN nanocolumn ensemble. The experimental data show three observable peaks: GaN(0002) at 34.56°, low-Al content AlGaN(0002) at 35.18°, and high-Al content AlGaN(0002) at 35.98°. Assuming that the nanocolumns are unstrained, manual fitting (keeping the segment structure but changing the composition) of the simulation model to the experimental data indicates that the Al molar fractions of the axial segments are 0, ∼0.43, and ∼0.97. Table 1 further elaborates the segment composition of the resulting fit for each segment in the nanocolumn structure.

Table 1. Al Content of Each Axial Nanocolumn Segment for the Vertical GaN/AlGaN Nanocolumn Ensemble (Top−Bottom) Obtained from Fitting the Simulation Model to the HRXRD $2\theta-\omega$ Scan Data

Segment	Thickness (nm)	Al bottom (%)	Al top (%)
p-GaN	38	0	0
p-AlGaN (linear grading)	190	46	40
i-GaN quantum disk	2	0	0
n-AlGaN (linear grading)	130	98	96
n-GaN	130	0	0
n-AlN buffer layer	25	100	100

Generally, the simulation result presented in Figure 1d fits relatively well with the $2\theta-\omega$ measurement, particularly for the high-Al content AlGaN(0002) reflection at 35.98°, where the Al content in this 130 nm-thick n-AlGaN segment has slight variation along the growth axis. A similar Al grading phenomenon is noticed for the low-Al content AlGaN(0002) peak at 35.18°, whose contribution comes from the 190 nm-thick p-AlGaN segment. In addition to the previous peaks, a GaN(0002) reflection at 34.56° is observed, originating from the n-GaN and p-GaN segments. Compared to their corresponding simulation results, a broadening in the experimental data of low-Al content AlGaN(0002) and GaN(0002) reflections is noted, probably due to strain in the vicinity of the interfaces that is not included in the simulation. Please note that the high Al content (∼0.97, from Table 1) in the n-AlGaN segment was unintentional and due to an insufficient control of the Al-to-Ga flux ratio during the synthesis of this segment. This growth calibration error was likely due to the high Ga desorption rate that was induced by the excessively high substrate temperature utilized during the formation of the n-AlGaN segment to reduce the coalescence effect between nanocolumns.

Structural characterizations of the nanocolumns and their interface with the graphene/silica glass substrate were further investigated by means of TEM. An overview of a number of self-assembled GaN/AlGaN nanocolumns grown on graphene is presented in the bright-field TEM (BFTEM) image in Figure 2a. The red arrow points at one specific nanocolumn for which the electron beam is parallel to the [1−210] crystal direction. Generally, all nanocolumns exhibit a single-crystalline wurtzite crystal structure and are grown along the *c*-axis, that is, [0001] direction, which is exemplified from an electron diffraction pattern (inset) taken from a nanocolumn oriented on the [1−210] zone axis. The high-angle annular dark-field (HAADF) STEM image in Figure 2b shows several layers inside the nanocolumns due to the contrast differences caused by the variations in the Ga/Al ratio. In HAADF STEM images, the contrast scales almost proportionally to the square of the atomic number (Z^2), that is, heavy atoms give bright contrast, and light atoms give dark contrast. Hence, this *Z*-contrast image presents the qualitative composition of the GaN/AlGaN nanocolumns.

Direct interpretation of the contrast differences depicted in Figure 2b suggests that the p-AlGaN segment has much lower Al content than the n-AlGaN segment. Between these two segments, the i-GaN quantum disk can be observed as a very thin layer (see also the HAADF image in Figure S4), having the same contrast as the p-GaN layer at the very top. The segments of the nominal n-GaN template (below the n-AlGaN segments) are seen to have a similar contrast as the p-AlGaN segments, which will be explained later. At the base of the nanocolumns, the n-AlN buffer layer grown using the two-stage deposition method tends to form a continuous layer, validating the previous SEM observation and corroborating the finding in our previous work.[40] While graphene in general is observed between the n-AlN buffer layer and silica glass support, a highly diffused interface with the n-AlN buffer layer is noticed in a few areas (e.g., blue arrow in Figure 2b), which might be due to poor graphene quality or surface damage of the fused silica wafer. Nanocolumns that originated from such areas tend to be randomly oriented (other examples can be seen in Figure S4).

The high-resolution HAADF STEM image in Figure 2c reveals the presence of graphene (dark contrast) with an approximate thickness of 0.34 nm (bottom-inset) located between the n-AlN buffer layer and silica glass support. Diffraction contrasts, that is, BFTEM images highlighting the existence of graphene and the elemental mapping from the interface region, are shown in Figure S5. Along with an identification of single-layer graphene from the C map, an Al signal is unexpectedly evident beneath the graphene. This might be due to intercalation, where Al atoms penetrate through defects or holes in the graphene during the growth of the AlN buffer layer. Apart from this, the graphene/n-AlN heterointerface is sharp and abrupt, indicating suppressed defect generation and high growth quality of the n-AlN buffer layer. The wurtzite crystal stacking sequence is observed in AlN with an interplanar lattice spacing of ∼0.50 nm (top-inset) along the vertical axis of the nanocolumn, which is in good agreement with the reported value for the *c*-axis direction of a wurtzite AlN crystal, thus further confirming the [0001] growth direction of the buffer layer.

The HAADF STEM image and elemental mapping of GaN/AlGaN nanocolumns from a different area of the same sample are presented in Figure 2d. The compositional analysis by EELS and EDS reveals that the nanocolumns consist of n-(Al)GaN/n-AlGaN/i-GaN quantum disk/p-AlGaN/p-GaN segments on top of the n-AlN buffer layer, wherein the average Al contents in n-AlGaN and p-AlGaN segments are 96 and 96%, respectively (individual elemental concentration distribution and the EDS line scan profile are shown in Figure S6-1 and Figure S6-2, respectively). Considering that EDS and EELS are semi-quantitative techniques, the chemical compositions determined from TEM are in line with those from HRXRD results. Nevertheless, one should be aware that the chemical composition interpretations from TEM give compositional variations inside single nanocolumns, whereas the XRD scan has the capability to probe a much larger number of nanocolumns in a single scan and thus provide average composition values for dominant nanocolumn segments (i.e., n- and p-AlGaN). Note that one of the nanocolumns in Figure

https://doi.org/10.1021/acsanm.1c02050
ACS Appl. Nano Mater. 2021, 4, 9653−9664

2d seems to have two i-GaN quantum disk layers. This is most likely due to contributions from two nanocolumns with slightly different heights (possibly, one of them is somewhat tilted) superposed on each other in the STEM image.

Due to a lower n-GaN stem density than that in our previous work[40] (since, nominally, the same growth conditions were applied, it is most likely caused by the differences in the graphene quality), n-AlGaN is deposited randomly on the n-AlN buffer layer during the formation of the n-AlGaN nanocolumns (96% Al). The profile of the n-AlGaN grown directly on the n-AlN buffer layer can be described as a rough layer with hillock-like structures of varying heights, due to the substrate rotation and shadowing from the randomly grown nanocolumns. Examples of such a structure can be seen on the right side of and around the base of the EDS-scanned nanocolumn on the top right panel in Figure S6-1. During the growth of the n-AlGaN (core) segment, an n-AlGaN shell is formed additionally on the n-GaN stem segment. As a result, the EDS line scan (Figure S6-2) shows an overlapped region in the base of the nominal n-GaN segment, where the Al signal is higher than the Ga signal due to the contribution from both the n-AlGaN hillock and the n-GaN/n-AlGaN core−shell nanocolumn. With regards to the Al-rich radial nanocolumn shell, it is observed (Figures 2d and S6-1) that such a shell also encloses almost the entire nanocolumns (except the top p-GaN segment part), which might act as a self-passivation layer for the nanocolumn side facets.

A representative HAADF STEM image of the i-GaN quantum disk region and its elemental mapping in Figure 2e disclose the non-faceted feature of the quantum disk layer (marked with a white dashed contour) situated between the n-$Al_{0.96}Ga_{0.04}N$ layer below and the p-$Al_{0.33}Ga_{0.67}N$ layer above. Particularly for the latter, it is unveiled that there are subtle compositional variations of Al-to-Ga composition ratios within the p-AlGaN section in the field of observation (individual elemental concentration distribution and the EDS line scan profile are presented in Figure S7), which can contribute to the broadening in the HRXRD $2\theta-\omega$ scan peak at 35.18° (Figure 1d). Because of the i-GaN quantum disk morphology (being very thin and not faceted), the measured composition ends up being a mixture of the composition in the intrinsic layer and the AlGaN layers in its immediate proximity, especially in the center area. It implies that the Ga content in the i-GaN quantum disk layer is likely to be underestimated; thus, it is difficult to deduce its chemical composition based on the compositional analysis alone. However, based on the contrast in the HAADF STEM images, it is reasonable to assume that the quantum disk layer is close to pure GaN. General interpretation of the i-GaN quantum disk is illustrated in the bottom image of Figure 2e, where the thickness of the quantum disk region in the center of the nanocolumn is less than that at its sides, being about 1.5 and 3 nm, respectively.

The HAADF STEM image in Figure 2f reveals a lattice-resolved image of the area in the vicinity of the i-GaN quantum disk region (only left part; the complete HAADF STEM image is depicted in Figure S8), where the i-GaN quantum disk layer is indicated by the white dashed contour. Like the i-GaN quantum disk, the p-AlGaN and n-AlGaN segments grow along the *c*-axis, adopting the wurtzite crystal structure. Furthermore, the interfaces between the p-AlGaN, i-GaN quantum disk, and n-AlGaN are observed without any noticeable defects (e.g., free of boundary or interface defects, threading dislocations, and stacking faults). An interplanar $d_{(0001)}$ spacing of around 0.52 nm is measured along the axial direction of the wurtzite i-GaN quantum disk (inset).

Figure 3 demonstrates a typical room temperature photoluminescence spectrum ranging from 280 to 658 nm of the as-grown GaN/AlGaN nanocolumn sample. A prominent emission band with a peak at around 300 nm is consistent with the Al composition of the top of the p-AlGaN section, which is around 40% (Table 1). The low-power spectrum (1 mW; Figure S9a) reveals that this emission consists of two overlapping peaks. This may be due to some contribution from defect-related levels in the p-AlGaN. No emission from the n-AlGaN segment is observed since its wavelength (~213 nm) is much shorter than the laser excitation wavelength (~260 nm). A Gaussian least-square fitting method reveals three peaks within the 325−420 nm wavelength region (Figure S9b), indicating that there are several contributions to the spectrum, including the i-GaN quantum disk and the p-GaN top segment. The absence of yellow and green luminescence bands that are typically present in the 500−600 nm range suggests a low defect density. Figure S9c presents the temperature dependence of the integrated photoluminescence intensity for three different excitation powers. The integrated photoluminescence intensity in the range of 325−420 nm at room temperature is 23.1% of the value at 10 K (at an excitation power of 10 mW, see Figure S9d), indicating additional contributions from non-radiative defects at room temperature.

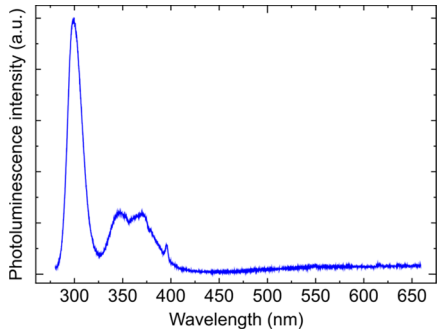

Figure 3. Room temperature photoluminescence spectrum of the GaN/AlGaN nanocolumn sample at an excitation power of 10 mW. Note that the sharp peak at ~395 nm is an artifact, presumably due to the scattered light from the graphene/silica interface region causing some interference or reflection.

Room temperature photoluminescence spectra of the GaN/AlGaN nanocolumn sample in Figures 3 and S9a clearly show that the emission from p-AlGaN is more dominant compared to emission from the i-GaN quantum disk and p-GaN, indicating limited diffusion of excited charge carriers from the p-AlGaN segment to the p-GaN top segment and the i-GaN quantum disk. Due to the longer segment length of p-AlGaN (~190 nm) as compared to that of p-GaN (~38 nm), most of the excitation light (260 nm laser light) will be absorbed in the p-AlGaN. A rough calculation (thin-film approximation, using absorption coefficients for GaN and AlGaN with 40% Al composition[62]) shows that less than 5% of the excitation light entering the top of the nanocolumn will reach the i-GaN quantum disk. In addition, around 30% of the photoluminescence from the i-GaN quantum disk propagating back along the nanocolumn toward the detector will be absorbed in the p-GaN top segment. However, considering

https://doi.org/10.1021/acsanm.1c02050
ACS Appl. Nano Mater. 2021, 4, 9653−9664

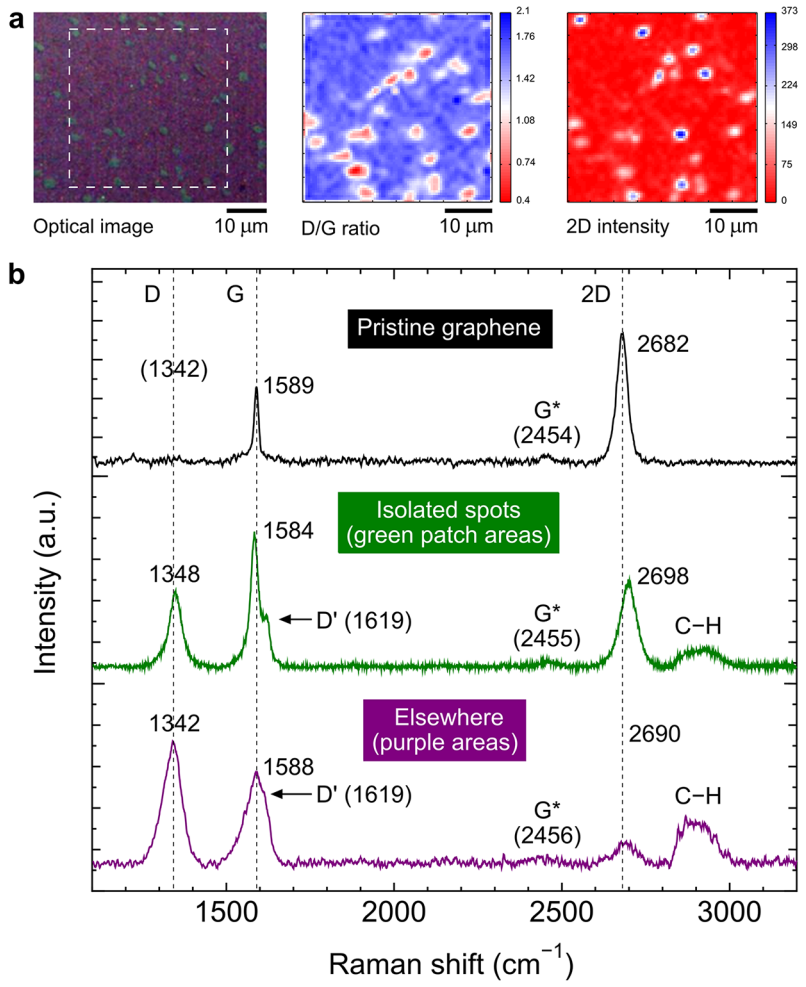

Figure 4. (a) Optical image and its corresponding micro-Raman D/G ratio and 2D intensity maps (from the area within the dashed square) of the graphene after the nanocolumn growth. (b) Raman spectra of graphene before and after nanocolumn growth.

that these GaN/AlGaN nanocolumns are not coalesced at the top, there is a likelihood that additional laser excitations can take place through the nanocolumn sidewalls and that additional emitted light (from the i-GaN quantum disks) can propagate between the nanocolumns to the detector. In addition, some diffusion of charge carriers from the p-AlGaN segment to the i-GaN quantum disk could enhance the photoluminescence from the latter. All in all, it is reasonable to expect that there is less photoluminescence intensity from the i-GaN quantum disks as compared to that from the p-GaN top segments.

Graphene's structural properties after the nanocolumn growth were evaluated using micro-Raman spectroscopy. Figure 4a shows an optical image and Raman mapping images of the graphene after the nanocolumn growth, with the dashed square on the optical image representing the area probed for the D/G ratio and 2D Raman intensity maps. In these images, a number of isolated spots (patches) are observed across the graphene, which differ from their surroundings. Interestingly, their appearance in the optical image is shown approximately at the same positions as map locations with a low D/G ratio and high 2D intensity. Based on this fact, it is very likely that the green spots on the optical image are actually the patch areas in the D/G ratio and 2D intensity maps. Furthermore, it is revealed that the graphene in these regions shows less damage than in the surrounding area, that is, indicated with relatively low D/G ratio and high 2D intensity values. With the growth taking place on single-layer graphene, it is expected that the damage to graphene will be more severe compared to that in nanocolumn growth on double-layer graphene,[40] and thus, the observed spots of higher graphene quality in this work could be due to multilayer patches that are present in graphene from the beginning.[63]

Figure 4b presents the comparison of the representative Raman spectra between the pristine graphene, patch areas, and elsewhere. The damage in the graphene after nanocolumn growth is obvious: the peak intensity of the defect-related D band at ∼1345 cm^{-1} is enhanced, whereas the peak intensities of the G and 2D bands at ∼1583 and ∼2686 cm^{-1} are reduced (the average D/G-ratio is found to be 1.52). In addition, another defect-related peak termed as the D′ peak at around 1619 cm^{-1} arises, which for most locations merges with the G peak and is seen as a shoulder. For the multilayer graphene patches, the aforementioned features are not as prominent as for the single-layer graphene regions. (We refer to Table S2 for a summary of additional micro-Raman spectroscopy measurements and Figure S10 for the corresponding maps and the averaged Raman spectra from different areas.) Regardless of these two different regions in the graphene after the growth, van der Pauw measurements show a sheet resistance of 4325

https://doi.org/10.1021/acsanm.1c02050
ACS Appl. Nano Mater. 2021, 4, 9653−9664

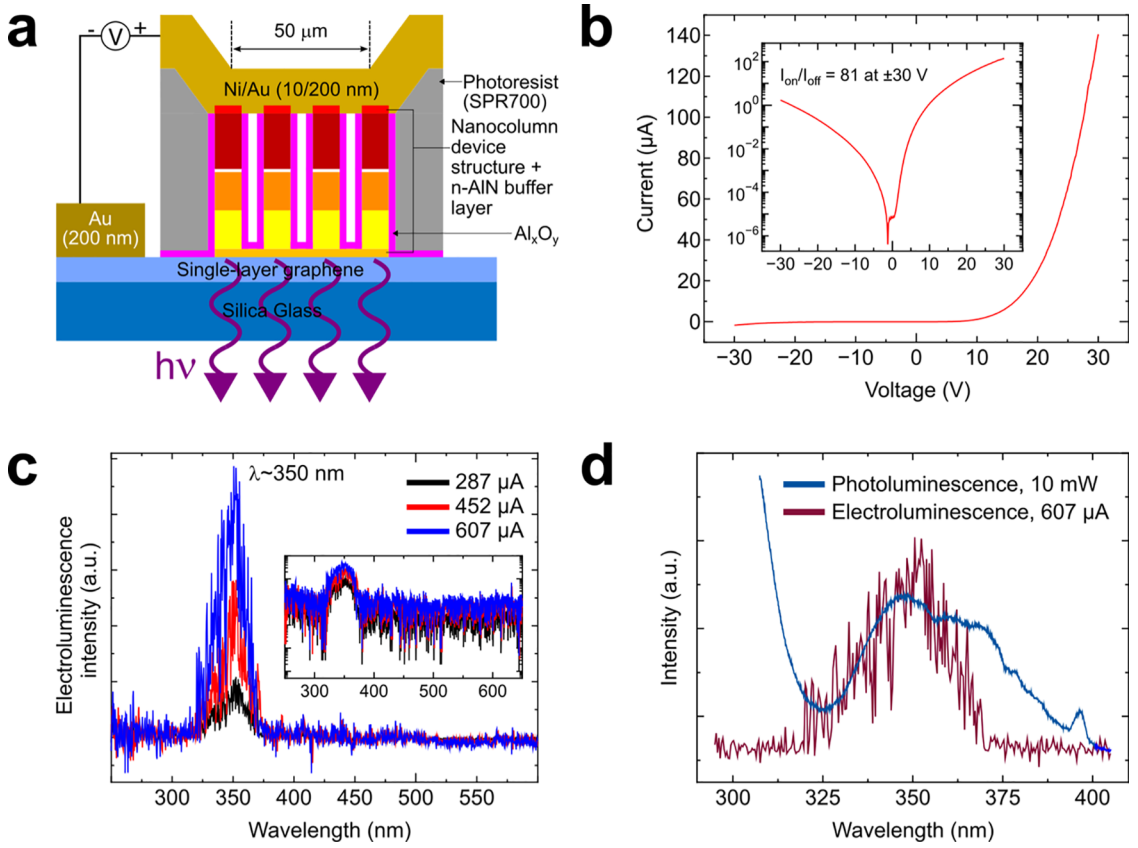

Figure 5. (a) Schematic representation of the GaN/AlGaN nanocolumn-based LED device, showing the light emission through the graphene/fused silica substrate in a flip-chip configuration. (b,c) Dark mode *I*−*V* characteristic and recorded electroluminescence spectra from a device with a 50 μm aperture diameter, along with their log scale presented in the respective insets. (d) Spectra from photoluminescence and electroluminescence measurements. The electroluminescence spectrum is fitted within the photoluminescence spectrum of interest for better visualization.

Ω/□, whereas it was measured to be 779 Ω/□ before growth.[40] Further growth studies of the AlN buffer layer on graphene are required to achieve less degradation in the graphene structural qualities while maintaining the verticality of GaN/AlGaN nanocolumns. One suggestion is by first depositing AlN on graphene in a non-plasma-dependent environment, such as MOVPE or ammonia-MBE. Alternatively, a selective area growth technique can be used,[11,19,38] such that the employed mask (e.g., Ti or SiO_2) protects most of the graphene areas from the direct exposure of the nitrogen plasma during the RF-PAMBE growth.

In order to demonstrate the application of graphene as a transparent conducting substrate, the nanocolumn sample was fabricated into an LED device, as schematically shown in Figure 5a. With this particular device configuration, the light is emitted through the transparent graphene/silica glass substrate as a flip-chip-type device. Here, the graphene transparent electrode allows a vertical current injection through the nanocolumn device structures. It is expected that the thick top metal contact uniformly connects the p-GaN nanocolumn layer in the defined contact area.

The current−voltage characteristics of a 50 μm-aperture diameter LED are presented in Figure 5b, revealing diode behavior with a rectification ratio of ∼81 at ± 30 V. However, the turn-on voltage is measured to be around 10 V (with a current of 1.2 μA), which is larger than that of similar GaN/AlGaN nanocolumn LEDs not utilizing graphene as a substrate and/or electrode.[64] One might expect that the high turn-on voltage is caused by a remaining thin insulating film of not completely etched Al_xO_y in the p-GaN region and/or surface damage in p-GaN during the process of oxide plasma etching of the Al_xO_y insulating layer. In conjunction with these issues, a preliminary device fabrication of the same GaN/AlGaN nanocolumn structure without the Al_xO_y layer has been performed (the device schematic and current−voltage characteristic are presented in Figure S11). Despite the fact that the Al_xO_y dielectric layer is not utilized, this processed nanocolumn device demonstrated a slightly higher turn-on voltage of approximately 12.5 V (with a current of 1.2 μA), compared to the presented value for the nanocolumn device using the Al_xO_y layer. This implies that the origin of such a high turn-on voltage observed in these nanocolumn-based LEDs using graphene as a transparent conducting substrate is not due to a remnant of the Al_xO_y layer and/or plasma damage in p-GaN but rather caused by other factors, as discussed below.

Considering that p-AlGaN and particularly n-AlGaN segments have very high Al content, a rather high turn-on voltage is anticipated for the LED device measured in this work. It is also observed that the increment of the current above the turn-on voltage is relatively slow, indicating a large device series resistance. Furthermore, the high sheet resistance of graphene leads to a much lower current at the same injection voltage compared to that in our previous work.[40] The usage of n-AlN as a buffer layer could be another factor contributing to the large resistance in the device due to an increased Schottky

https://doi.org/10.1021/acsanm.1c02050
ACS Appl. Nano Mater. 2021, 4, 9653−9664

barrier height (see Figure 3.5 in ref 58) and low doping density. (It should be noted that although n-AlN is a highly resistive material, defect inclusions in AlN likely provide a short-circuit path for electron injection from the graphene into the n-GaN.[65,66]) A dedicated study is needed to confirm the nature of the Schottky barrier interface in the graphene/n-AlN/n-GaN. Furthermore, the development of an optimized buffer layer growth method is therefore required to improve the performance of the vertical nanocolumn LEDs using graphene as a transparent conducting substrate, for example, using an n-AlGaN buffer layer (low Al content) or a short-period n-AlN/n-AlGaN superlattice buffer[67,68] to obtain vertical nanocolumn structures while maintaining a sufficiently low LED operating voltage.

The electroluminescence spectra of the LED device measured at room temperature are presented in Figure 5c, with a peak emission at ∼350 nm, which is within the 325−420 nm wavelength region of the GaN-related photoluminescence emission from the same sample (Figure 5d). The electroluminescence peak emission is blue-shifted from the common 365 nm band gap of bulk undoped wurtzite GaN. This is most likely due to the quantum confinement effect on both electrons and holes in the 1D quantum potential[69] of the i-GaN quantum disk (shown in Figure 2f) since a significant fraction of this region has a thickness within the range of the reported exciton Bohr radius for GaN,[69,70] that is, between 2.8 and 11 nm, in combination with the effect of strain in the i-GaN quantum disk due to the surrounding AlGaN.[71] As evidenced by the log scale in the inset of Figure 5c, a defect-related broad yellow luminescence band is not detected (as was also the case in the photoluminescence measurements described above), indicating that structural defects such as threading dislocations and stacking faults are not present in the grown GaN/AlGaN nanocolumn device structure. Also, no electroluminescence is detected at or beyond 370 nm, indicating that the injected electrons are not reaching the p-GaN segments (i.e., no "electron overshooting").

One should note here that the electroluminescence spectra in Figure 5c,d are the measurement results of light that is emitted through the graphene/silica glass substrate. Around 70% of the electroluminescence emission from the i-GaN quantum disk propagating in the nanocolumn toward the graphene/silica glass substrate is absorbed in the 130 nm-long n-GaN segment, due to the higher photon energy (∼3.54 eV) of the emission from the i-GaN quantum disk as compared to the band gap of n-GaN (3.39 eV). Therefore, an important issue to be considered for the future nanocolumn-based flip-chip LEDs on graphene is the absorption of UV light (whose wavelength is shorter than 365 nm) by the long n-GaN nanocolumn template.[72,73] In order to improve the light output of this particular flip-chip LED device, a shorter n-GaN nanocolumn template or preferably an n-AlGaN nanocolumn template transparent to the emitted UV light from the active region should be utilized.

CONCLUSIONS

RF-PAMBE growth of high-density vertical GaN/AlGaN nanocolumns on single-layer graphene (transferred onto fused silica glass) is demonstrated by means of a two-stage AlN buffer layer deposition method. TEM indicates that the nanocolumns are of high crystalline quality and shows the formation of an intrinsic GaN quantum disk layer between the axial n- and p-AlGaN segments. Photoluminescence characterization notes the emission peaks from the different regions in the nanocolumn structure, including an emission around 350 nm originating from the i-GaN quantum disk layer. No yellow luminescence emission is observed from the photoluminescence spectrum. Micro-Raman spectroscopy shows that the graphene is severely damaged after the RF-PAMBE nanocolumn growth, and the resulting high graphene sheet resistance causes a rather high turn-on voltage in a fabricated flip-chip LED device. Nevertheless, the concept of single-layer graphene simultaneously utilized as a substrate for the nanocolumn growth and a transparent bottom electrode has been demonstrated. Electroluminescence emission from the LED device evidences a peak emission at ∼350 nm from the i-GaN nanocolumn quantum disk with no defect-related yellow emission. This blue shift from typical bulk wurtzite GaN emission at ∼365 nm is believed to be due to the quantum confinement effect and strain in the i-GaN quantum disk.

ASSOCIATED CONTENT

Supporting Information

The Supporting Information is available free of charge at https://pubs.acs.org/doi/10.1021/acsanm.1c02050.

Additional SEM and TEM images of the relevant nanocolumn growth results on graphene and further photoluminescence, micro-Raman, and $I-V$ measurements (PDF)

AUTHOR INFORMATION

Corresponding Authors

Katsumi Kishino − *Department of Engineering and Applied Sciences, Sophia University, Tokyo 102-8554, Japan; Sophia Nanotechnology Research Center, Sophia University, Tokyo 102-8554, Japan*; Email: kishino@sophia.ac.jp

Bjørn-Ove Fimland − *Department of Electronic Systems, Norwegian University of Science and Technology (NTNU), Trondheim NO-7491, Norway*; Email: bjorn.fimland@ntnu.no

Authors

Andreas Liudi Mulyo − *Department of Electronic Systems, Norwegian University of Science and Technology (NTNU), Trondheim NO-7491, Norway; Department of Engineering and Applied Sciences, Sophia University, Tokyo 102-8554, Japan*; orcid.org/0000-0002-7323-7661

Anjan Mukherjee − *Department of Electronic Systems, Norwegian University of Science and Technology (NTNU), Trondheim NO-7491, Norway*

Ida Marie Høiaas − *Department of Electronic Systems, Norwegian University of Science and Technology (NTNU), Trondheim NO-7491, Norway*

Lyubomir Ahtapodov − *Department of Electronic Systems, Norwegian University of Science and Technology (NTNU), Trondheim NO-7491, Norway*

Tron Arne Nilsen − *Department of Electronic Systems, Norwegian University of Science and Technology (NTNU), Trondheim NO-7491, Norway*

Håvard Hem Toftevaag − *Department of Electronic Systems, Norwegian University of Science and Technology (NTNU), Trondheim NO-7491, Norway*

Per Erik Vullum − *SINTEF Industry, Trondheim NO-7465, Norway; Department of Physics, Norwegian University of*

https://doi.org/10.1021/acsanm.1c02050
ACS Appl. Nano Mater. 2021, 4, 9653−9664

Science and Technology (NTNU), Trondheim NO-7491, Norway

Helge Weman − *Department of Electronic Systems, Norwegian University of Science and Technology (NTNU), Trondheim NO-7491, Norway;* orcid.org/0000-0001-5470-9953

Complete contact information is available at: https://pubs.acs.org/10.1021/acsanm.1c02050

Author Contributions

A.M and I.M.H contributed equally to this study. A.L.M planned the experiments under the supervision of B.-O.F, H.W, and K.K. A.L.M performed the nanocolumn growth by MBE and SEM imaging. I.M.H and H.H.T conducted Raman spectroscopy and mapping and analyzed the data, in collaboration with A.L.M. I.M.H. and A.M carried out preliminary device fabrication and *I*−*V* measurements, while A.M fabricated the final LED device together with H.H.T and did *I*−*V*/EL measurements. T.A.N did XRD characterization, simulation, and analysis. P.E.V performed TEM/STEM/EDX/EELS imaging and spectroscopy. L.A conducted the photoluminescence measurements and analysis. A.L.M drafted the manuscript. All authors contributed to the discussion of results and preparations of the manuscript.

Notes

The authors declare no competing financial interest.

■ ACKNOWLEDGMENTS

The authors wish to thank D. L. Dheeraj of CrayoNano and D.-C. Kim of NTNU for fruitful discussions. Technical MBE support, maintenance, and insightful suggestions from K. Yamano, I. Matsuyama, S. Ishizawa, Y. Nakagawa, and Y. Matsui of Sophia University are appreciated as well. In addition, we also appreciate the assistance from Prof. Kawakami's group of Kyoto University for initial photoluminescence measurements. We acknowledge the financial support from the Research Council of Norway through NANO2021 program (grant no. 259553) and the Japan Society for the Promotion of Science KAKENHI (grant no. 19H00874). The Research Council of Norway is acknowledged for the support to the Norwegian Micro- and Nano-Fabrication Facility, NorFab (grant no. 295864), the Norwegian Center for Transmission Electron Microscopy, NORTEM (grant no. 197405/F50), and the Norwegian PhD Network on Nanotechnology for Microsystems, FORSKERSKOLER (grant no. 221860/F60). NTNU Nano is acknowledged for support through the NTNU Nano Impact Fund.

■ REFERENCES

(1) Park, J.-H.; Nandi, R.; Sim, J.-K.; Um, D.-Y.; Kang, S.; Kim, J.-S.; Lee, C.-R. A III-nitride nanowire solar cell fabricated using a hybrid coaxial and uniaxial InGaN/GaN multi quantum well nanostructure. *RSC Adv.* **2018**, *8*, 20585−20592.

(2) Cheriton, R.; Sadaf, S. M.; Robichaud, L.; Krich, J. J.; Mi, Z.; Hinzer, K. Two-photon photocurrent in InGaN/GaN nanowire intermediate band solar cells. *Commun.Commun.* **2020**, *1*, 63.

(3) Wang, Y.; Vanka, S.; Gim, J.; Wu, Y.; Fan, R.; Zhang, Y.; Shi, J.; Shen, M.; Hovden, R.; Mi, Z. An In0.42Ga0.58N tunnel junction nanowire photocathode monolithically integrated on a nonplanar Si wafer. *Nano Energy* **2019**, *57*, 405−413.

(4) Yu, F.; Yao, S.; Römer, F.; Witzigmann, B.; Schimpke, T.; Strassburg, M.; Bakin, A.; Schumacher, H. W.; Peiner, E.; Wasisto, H. S.; Waag, A. GaN nanowire arrays with nonpolar sidewalls for vertically integrated field-effect transistors. *Nanotechnology* **2017**, *28*, 095206.

(5) Song, W.; Wang, R.; Wang, X.; Guo, D.; Chen, H.; Zhu, Y.; Liu, L.; Zhou, Y.; Sun, Q.; Wang, L.; Li, S. a-Axis GaN/AlN/AlGaN Core-Shell Heterojunction Microwires as Normally Off High Electron Mobility Transistors. *ACS Appl. Mater. Interfaces* **2017**, *9*, 41435−41442.

(6) Sun, R.; Wang, G.-G.; Peng, Z.-C. Fabrication and UV photoresponse of GaN nanowire-film hybrid films on sapphire substrates by chemical vapor deposition method. *Mater. Lett.* **2018**, *217*, 288−291.

(7) Aiello, A.; Hoque, A. K. M. H.; Baten, M. Z.; Bhattacharya, P. High-Gain Silicon-Based InGaN/GaN Dot-in-Nanowire Array Photodetector. *ACS Photonics* **2019**, *6*, 1289−1294.

(8) Ra, Y.-H.; Rashid, R. T.; Liu, X.; Sadaf, S. M.; Mashooq, K.; Mi, Z. An electrically pumped surface-emitting semiconductor green laser. *Sci. Adv.* **2020**, *6*, No. eaav7523.

(9) Kishino, K.; Ishizawa, S. Spectrally-broadened multimode lasing based on structurally graded InGaN nanocolumn photonic crystals suitable for reduction of speckle contrast. *Appl. Phys. Lett.* **2016**, *109*, 071106.

(10) Kishino, K.; Sakakibara, N.; Narita, K.; Oto, T. Two-dimensional multicolor (RGBY) integrated nanocolumn micro-LEDs as a fundamental technology of micro-LED display. *Appl. Phys. Express* **2019**, *13*, 014003.

(11) Yamano, K.; Kishino, K. Selective area growth of InGaN-based nanocolumn LED crystals on AlN/Si substrates useful for integrated μ-LED fabrication. *Appl. Phys. Lett.* **2018**, *112*, 091105.

(12) Wu, Y.; Wang, Y.; Sun, K.; Mi, Z. Molecular beam epitaxy and characterization of AlGaN nanowire ultraviolet light emitting diodes on Al coated Si (0 0 1) substrate. *J. Cryst. Growth* **2019**, *507*, 65−69.

(13) Sukegawa, A.; Sekiguchi, H.; Matsuzaki, R.; Yamane, K.; Okada, H.; Kishino, K.; Wakahara, A. Self-Organized Eu-Doped GaN Nanocolumn Light-Emitting Diode Grown by RF-Molecular-Beam Epitaxy. *Phys. Status Solidi A* **2019**, *216*, 1800501.

(14) Liu, X.; Wu, Y.; Malhotra, Y.; Sun, Y.; Mi, Z. Micrometer scale InGaN green light emitting diodes with ultra-stable operation. *Appl. Phys. Lett.* **2020**, *117*, 011104.

(15) Kavanagh, K. L. Misfit dislocations in nanowire heterostructures. *Semicond. Sci. Technol.* **2010**, *25*, 024006.

(16) Kishino, K.; Ishizawa, S. Selective-area growth of GaN nanocolumns on Si(111) substrates for application to nanocolumn emitters with systematic analysis of dislocation filtering effect of nanocolumns. *Nanotechnology* **2015**, *26*, 225602.

(17) Yamano, K.; Kishino, K.; Sekiguchi, H.; Oto, T.; Wakahara, A.; Kawakami, Y. Novel selective area growth (SAG) method for regularly arranged AlGaN nanocolumns using nanotemplates. *J. Cryst. Growth* **2015**, *425*, 316−321.

(18) Wu, Y.; Wang, Y.; Sun, K.; Aiello, A.; Bhattacharya, P.; Mi, Z. Molecular beam epitaxy and characterization of Mg-doped GaN epilayers grown on Si (0 0 1) substrate through controlled nanowire coalescence. *J. Cryst. Growth* **2018**, *498*, 109−114.

(19) Oto, T.; Mizuno, Y.; Yamano, K.; Yoshida, J.; Kishino, K. Column diameter dependence of the strain relaxation effect in GaN/AlGaN quantum wells on GaN nanocolumn arrays. *Appl. Phys. Express* **2019**, *12*, 125001.

(20) Wu, Y.; Liu, B.; Li, Z.; Tao, T.; Xie, Z.; Wang, K.; Xiu, X.; Chen, D.; Lu, H.; Zhang, R.; Zheng, Y. The influence of an AlN seeding layer on nucleation of self-assembled GaN nanowires on silicon substrates. *Nanotechnology* **2019**, *31*, 045604.

(21) Eftychis, S.; Kruse, J. E.; Tsagaraki, K.; Koukoula, T.; Kehagias, T.; Komninou, P.; Georgakilas, A. Effects of ultrathin AlN prelayers on the spontaneous growth of GaN nanowires by plasma assisted molecular beam epitaxy. *J. Cryst. Growth* **2019**, *514*, 89−97.

(22) May, B. J.; Sarwar, A. T. M. G.; Myers, R. C. Nanowire LEDs grown directly on flexible metal foil. *Appl. Phys. Lett.* **2016**, *108*, 141103.

(23) Calabrese, G.; Corfdir, P.; Gao, G.; Pfüller, C.; Trampert, A.; Brandt, O.; Geelhaar, L.; Fernández-Garrido, S. Molecular beam epitaxy of single crystalline GaN nanowires on a flexible Ti foil. *Appl. Phys. Lett.* **2016**, *108*, 202101.
(24) Zhao, C.; Ng, T. K.; ElAfandy, R. T.; Prabaswara, A.; Consiglio, G. B.; Ajia, I. A.; Roqan, I. S.; Janjua, B.; Shen, C.; Eid, J.; Alyamani, A. Y.; El-Desouki, M. M.; Ooi, B. S. Droop-Free, Reliable, and High-Power InGaN/GaN Nanowire Light-Emitting Diodes for Monolithic Metal-Optoelectronics. *Nano Lett.* **2016**, *16*, 4616−4623.
(25) Ramesh, C.; Tyagi, P.; Gautam, S.; Ojha, S.; Gupta, G.; Kumar, M. S.; Kushvaha, S. S. Controlled growth of GaN nanorods directly on flexible Mo metal foil by laser molecular beam epitaxy. *Mater. Sci. Semicond. Process.* **2020**, *111*, 104988.
(26) Zhao, C.; Ng, T. K.; Tseng, C.-C.; Li, J.; Shi, Y.; Wei, N.; Zhang, D.; Consiglio, G. B.; Prabaswara, A.; Alhamoud, A. A.; Albadri, A. M.; Alyamani, A. Y.; Zhang, X. X.; Li, L.-J.; Ooi, B. S. InGaN/GaN nanowires epitaxy on large-area MoS2 for high-performance light-emitters. *RSC Adv.* **2017**, *7*, 26665−26672.
(27) Prabaswara, A.; Kim, H.; Min, J.-W.; Subedi, R. C.; Anjum, D. H.; Davaasuren, B.; Moore, K.; Conroy, M.; Mitra, S.; Roqan, I. S.; Ng, T. K.; Alshareef, H. N.; Ooi, B. S. Titanium Carbide MXene Nucleation Layer for Epitaxial Growth of High-Quality GaN Nanowires on Amorphous Substrates. *ACS Nano* **2020**, *14*, 2202−2211.
(28) Schuster, F.; Hetzl, M.; Weiszer, S.; Wolfer, M.; Kato, H.; Nebel, C. E.; Garrido, J. A.; Stutzmann, M. Optoelectronic properties of p-diamond/n-GaN nanowire heterojunctions. *J. Appl. Phys.* **2015**, *118*, 154303.
(29) Sundaram, S.; Li, X.; Halfaya, Y.; Ayari, T.; Patriarche, G.; Bishop, C.; Alam, S.; Gautier, S.; Voss, P. L.; Salvestrini, J. P.; Ougazzaden, A. Large-Area van der Waals Epitaxial Growth of Vertical III-Nitride Nanodevice Structures on Layered Boron Nitride. *Adv. Mater. Interfaces* **2019**, *6*, 1900207.
(30) Sobanska, M.; Zytkiewicz, Z. R.; Klosek, K.; Kruszka, R.; Golaszewska, K.; Ekielski, M.; Gieraltowska, S. Selective area formation of GaN nanowires on GaN substrates by the use of amorphous Al x O y nucleation layer. *Nanotechnology* **2020**, *31*, 184001.
(31) Kumaresan, V.; Largeau, L.; Oehler, F.; Zhang, H.; Mauguin, O.; Glas, F.; Gogneau, N.; Tchernycheva, M.; Harmand, J.-C. Self-induced growth of vertical GaN nanowires on silica. *Nanotechnology* **2016**, *27*, 135602.
(32) Li, H.; Zhao, G.; Wei, H.; Wang, L.; Chen, Z.; Yang, S. Growth of Well-Aligned InN Nanorods on Amorphous Glass Substrates. *Nanoscale Res. Lett.* **2016**, *11*, 270.
(33) Liudi Mulyo, A.; Konno, Y.; Nilsen, J. S.; van Helvoort, A. T. J.; Fimland, B.-O.; Weman, H.; Kishino, K. Growth study of self-assembled GaN nanocolumns on silica glass by plasma assisted molecular beam epitaxy. *J. Cryst. Growth* **2017**, *480*, 67−73.
(34) Prabaswara, A.; Min, J.-W.; Zhao, C.; Janjua, B.; Zhang, D.; Albadri, A. M.; Alyamani, A. Y.; Ng, T. K.; Ooi, B. S. Direct Growth of III-Nitride Nanowire-Based Yellow Light-Emitting Diode on Amorphous Quartz Using Thin Ti Interlayer. *Nanoscale Res. Lett.* **2018**, *13*, 41.
(35) Hayashi, H.; Konno, Y.; Kishino, K. Self-organization of dislocation-free, high-density, vertically aligned GaN nanocolumns involving InGaN quantum wells on graphene/SiO2 covered with a thin AlN buffer layer. *Nanotechnology* **2016**, *27*, 055302.
(36) Heilmann, M.; Munshi, A. M.; Sarau, G.; Göbelt, M.; Tessarek, C.; Fauske, V. T.; van Helvoort, A. T. J.; Yang, J.; Latzel, M.; Hoffmann, B.; Conibeer, G.; Weman, H.; Christiansen, S. Vertically Oriented Growth of GaN Nanorods on Si Using Graphene as an Atomically Thin Buffer Layer. *Nano Lett.* **2016**, *16*, 3524−3532.
(37) Fernández-Garrido, S.; Ramsteiner, M.; Gao, G.; Galves, L. A.; Sharma, B.; Corfdir, P.; Calabrese, G.; de Souza Schiaber, Z.; Pfüller, C.; Trampert, A.; Lopes, J. M. J.; Brandt, O.; Geelhaar, L. Molecular Beam Epitaxy of GaN Nanowires on Epitaxial Graphene. *Nano Lett.* **2017**, *17*, 5213−5221.
(38) Munshi, A. M.; Kim, D.-C.; Heimdal, C. P.; Heilmann, M.; Christiansen, S. H.; Vullum, P. E.; van Helvoort, A. T. J.; Weman, H. Selective area growth of AlGaN nanopyramid arrays on graphene by metal-organic vapor phase epitaxy. *Appl. Phys. Lett.* **2018**, *113*, 263102.
(39) Liudi Mulyo, A.; Rajpalke, M. K.; Kuroe, H.; Vullum, P.-E.; Weman, H.; Fimland, B.-O.; Kishino, K. Vertical GaN nanocolumns grown on graphene intermediated with a thin AlN buffer layer. *Nanotechnology* **2019**, *30*, 015604.
(40) Høiaas, I. M.; Liudi Mulyo, A.; Vullum, P. E.; Kim, D.-C.; Ahtapodov, L.; Fimland, B.-O.; Kishino, K.; Weman, H. GaN/AlGaN Nanocolumn Ultraviolet Light-Emitting Diode Using Double-Layer Graphene as Substrate and Transparent Electrode. *Nano Lett.* **2019**, *19*, 1649−1658.
(41) Zheng, Y.; Wang, W.; Li, Y.; Lan, J.; Xia, Y.; Yang, Z.; He, X.; Li, G. Self-Integrated Hybrid Ultraviolet Photodetectors Based on the Vertically Aligned InGaN Nanorod Array Assembly on Graphene. *ACS Appl. Mater. Interfaces* **2019**, *11*, 13589−13597.
(42) Wang, Y.; Dheeraj, D.; Liu, Z.; Liang, M.; Li, Y.; Yi, X.; Wang, J.; Li, J.; Weman, H. AlGaN Nanowires Grown on SiO2/Si (100) Using Graphene as a Buffer Layer. *Cryst. Growth Des.* **2019**, *19*, 5516−5522.
(43) Liudi Mulyo, A.; Rajpalke, M. K.; Vullum, P. E.; Weman, H.; Kishino, K.; Fimland, B.-O. The influence of AlN buffer layer on the growth of self-assembled GaN nanocolumns on graphene. *Sci. Rep.* **2020**, *10*, 853.
(44) Zulkifli, N. A. A.; Park, K.; Min, J.-W.; Ooi, B. S.; Zakaria, R.; Kim, J.; Tan, C. L. A highly sensitive, large area, and self-powered UV photodetector based on coalesced gallium nitride nanorods/graphene/silicon (111) heterostructure. *Appl. Phys. Lett.* **2020**, *117*, 191103.
(45) Jeong, J.; Wang, Q.; Cha, J.; Jin, D. K.; Shin, D. H.; Kwon, S.; Kang, B. K.; Jang, J. H.; Yang, W. S.; Choi, Y. S.; Yoo, J.; Kim, J. K.; Lee, C.-H.; Lee, S. W.; Zakhidov, A.; Hong, S.; Kim, M. J.; Hong, Y. J. Remote heteroepitaxy of GaN microrod heterostructures for deformable light-emitting diodes and wafer recycle. *Sci. Adv.* **2020**, *6*, No. eaaz5180.
(46) Mancini, L.; Morassi, M.; Sinito, C.; Brandt, O.; Geelhaar, L.; Song, H.-G.; Cho, Y.-H.; Guan, N.; Cavanna, A.; Njeim, J.; Madouri, A.; Barbier, C.; Largeau, L.; Babichev, A.; Julien, F. H.; Travers, L.; Oehler, F.; Gogneau, N.; Harmand, J.-C.; Tchernycheva, M. Optical properties of GaN nanowires grown on chemical vapor deposited-graphene. *Nanotechnology* **2019**, *30*, 214005.
(47) Morassi, M.; Guan, N.; Dubrovskii, V. G.; Berdnikov, Y.; Barbier, C.; Mancini, L.; Largeau, L.; Babichev, A. V.; Kumaresan, V.; Julien, F. H.; Travers, L.; Gogneau, N.; Harmand, J.-C.; Tchernycheva, M. Selective Area Growth of GaN Nanowires on Graphene Nanodots. *Cryst. Growth Des.* **2020**, *20*, 552−559.
(48) Liang, D.; Wei, T.; Wang, J.; Li, J. Quasi van der Waals epitaxy nitride materials and devices on two dimension materials. *Nano Energy* **2020**, *69*, 104463.
(49) Tran Khac, B.-C.; DelRio, F. W.; Chung, K.-H. Interfacial Strength and Surface Damage Characteristics of Atomically Thin h-BN, MoS2, and Graphene. *ACS Appl. Mater. Interfaces* **2018**, *10*, 9164−9177.
(50) Tangi, M.; Mishra, P.; Ng, T. K.; Hedhili, M. N.; Janjua, B.; Alias, M. S.; Anjum, D. H.; Tseng, C.-C.; Shi, Y.; Joyce, H. J.; Li, L.-J.; Ooi, B. S. Determination of band offsets at GaN/single-layer MoS2 heterojunction. *Appl. Phys. Lett.* **2016**, *109*, 032104.
(51) Petukhov, D. I.; Chumakov, A. P.; Kan, A. S.; Lebedev, V. A.; Eliseev, A. A.; Konovalov, O. V.; Eliseev, A. A. Spontaneous MXene monolayer assembly at the liquid-air interface. *Nanoscale* **2019**, *11*, 9980−9986.
(52) Wu, C.; Soomro, A. M.; Sun, F.; Wang, H.; Huang, Y.; Wu, J.; Liu, C.; Yang, X.; Gao, N.; Chen, X.; Kang, J.; Cai, D. Large-roll growth of 25-inch hexagonal BN monolayer film for self-release buffer layer of free-standing GaN wafer. *Sci. Rep.* **2016**, *6*, 34766.

https://doi.org/10.1021/acsanm.1c02050
ACS Appl. Nano Mater. 2021, 4, 9653−9664

(53) Xie, C.; Wang, Y.; Zhang, Z.-X.; Wang, D.; Luo, L.-B. Graphene/Semiconductor Hybrid Heterostructures for Optoelectronic Device Applications. *Nano Today* **2018**, *19*, 41−83.
(54) Gupta, P.; Rahman, A. A.; Subramanian, S.; Gupta, S.; Thamizhavel, A.; Orlova, T.; Rouvimov, S.; Vishwanath, S.; Protasenko, V.; Laskar, M. R.; Xing, H. G.; Jena, D.; Bhattacharya, A. Layered transition metal dichalcogenides: promising near-lattice-matched substrates for GaN growth. *Sci. Rep.* **2016**, *6*, 23708.
(55) Li, W.; Cheng, G.; Liang, Y.; Tian, B.; Liang, X.; Peng, L.; Hight Walker, A. R.; Gundlach, D. J.; Nguyen, N. V. Broadband optical properties of graphene by spectroscopic ellipsometry. *Carbon* **2016**, *99*, 348−353.
(56) Polat, E. O.; Balci, O.; Kakenov, N.; Uzlu, H. B.; Kocabas, C.; Dahiya, R. Synthesis of Large Area Graphene for High Performance in Flexible Optoelectronic Devices. *Sci. Rep.* **2015**, *5*, 16744.
(57) Gahoi, A.; Wagner, S.; Bablich, A.; Kataria, S.; Passi, V.; Lemme, M. C. Contact resistance study of various metal electrodes with CVD graphene. *Solid-State Electron.* **2016**, *125*, 234−239.
(58) Liudi Mulyo, A. Molecular Beam Epitaxy of GaN/AlGaN Nanocolumns on Graphene: For Potential Application in Ultraviolet Light-Emitting Diodes. Doctoral Thesis, Norwegian University of Science and Technology (NTNU), Trondheim, Norway, 2021. https://hdl.handle.net/11250/2759464.
(59) Jenichen, B.; Brandt, O.; Pfüller, C.; Dogan, P.; Knelangen, M.; Trampert, A. Macro- and micro-strain in GaN nanowires on Si(111). *Nanotechnology* **2011**, *22*, 295714.
(60) Fernández-Garrido, S.; Kaganer, V. M.; Hauswald, C.; Jenichen, B.; Ramsteiner, M.; Consonni, V.; Geelhaar, L.; Brandt, O. Correlation between the structural and optical properties of spontaneously formed GaN nanowires: a quantitative evaluation of the impact of nanowire coalescence. *Nanotechnology* **2014**, *25*, 455702.
(61) Kriegner, D.; Wintersberger, E.; Stangl, J. xrayutilities: a versatile tool for reciprocal space conversion of scattering data recorded with linear and area detectors. *J. Appl. Crystallogr.* **2013**, *46*, 1162−1170.
(62) Muth, J. F.; Brown, J. D.; Johnson, M. A. L.; Yu, Z.; Kolbas, R. M.; Cook, J. W.; Schetzina, J. F. Absorption Coefficient and Refractive Index of GaN, AlN and AlGaN Alloys. *MRS Internet J. Nitride Semicond. Res.* **1999**, *4*, 502−507.
(63) Han, Z.; Kimouche, A.; Kalita, D.; Allain, A.; Arjmandi-Tash, H.; Reserbat-Plantey, A.; Marty, L.; Pairis, S.; Reita, V.; Bendiab, N.; Coraux, J.; Bouchiat, V. Homogeneous Optical and Electronic Properties of Graphene Due to the Suppression of Multilayer Patches During CVD on Copper Foils. *Adv. Funct. Mater.* **2014**, *24*, 964−970.
(64) Sekiguchi, H.; Kato, K.; Tanaka, J.; Kikuchi, A.; Kishino, K. Ultraviolet GaN-based nanocolumn light-emitting diodes grown on n-(111) Si substrates by rf-plasma-assisted molecular beam epitaxy. *Phys. Status Solidi A* **2008**, *205*, 1067−1069.
(65) Guha, S.; Bojarczuk, N. A. Ultraviolet and violet GaN light emitting diodes on silicon. *Appl. Phys. Lett.* **1998**, *72*, 415−417.
(66) Tran, C. A.; Osinski, A.; Karlicek, R. F., Jr. Growth of InGaN/GaN multiple-quantum-well blue light-emitting diodes on silicon by metalorganic vapor phase epitaxy. *Appl. Phys. Lett.* **1999**, *75*, 1494−1496.
(67) Egawa, T.; Shuhaimi, B. A. B. A. High performance InGaN LEDs on Si (1 1 1) substrates grown by MOCVD. *J. Phys. D: Appl. Phys.* **2010**, *43*, 354008.
(68) Zhang, B.; Egawa, T.; Ishikawa, H.; Liu, Y.; Jimbo, T. High-Bright InGaN Multiple-Quantum-Well Blue Light-Emitting Diodes on Si (111) Using AlN/GaN Multilayers with a Thin AlN/AlGaN Buffer Layer. *Jpn. J. Appl. Phys.* **2003**, *42*, L226−L228.
(69) Liu, J.; Meng, X.-M.; Jiang, Y.; Lee, C.-S.; Bello, I.; Lee, S.-T. Gallium nitride nanowires doped with silicon. *Appl. Phys. Lett.* **2003**, *83*, 4241−4243.
(70) Ramvall, P.; Tanaka, S.; Nomura, S.; Riblet, P.; Aoyagi, Y. Observation of confinement-dependent exciton binding energy of GaN quantum dots. *Appl. Phys. Lett.* **1998**, *73*, 1104−1106.
(71) Reszka, A.; Wierzbicka, A.; Sobczak, K.; Jahn, U.; Zeimer, U.; Kuchuk, A. V.; Pieniążek, A.; Sobanska, M.; Klosek, K.; Zytkiewicz, Z. R.; Kowalski, B. J. An influence of the local strain on cathodoluminescence of GaN/AlxGa1−xN nanowire structures. *J. Appl. Phys.* **2016**, *120*, 194304.
(72) Jayaprakash, R.; Ajagunna, D.; Germanis, S.; Androulidaki, M.; Tsagaraki, K.; Georgakilas, A.; Pelekanos, N. T. Extraction of absorption coefficients from as-grown GaN nanowires on opaque substrates using all-optical method. *Opt. Express* **2014**, *22*, 19555−19566.
(73) Bao, Y.; Xu, S. Dopant-Induced Electric Fields and Their Influence on the Band-Edge Absorption of GaN. *ACS Omega* **2019**, *4*, 15401−15406.

https://doi.org/10.1021/acsanm.1c02050
ACS Appl. Nano Mater. 2021, 4, 9653−9664